Comput. Methods Appl. Mech. Engrg. 198 (2009) 2198–2208

Contents lists available at ScienceDirect

Comput. Methods Appl. Mech. Engrg.

journal homepage: www.elsevier.com/locate/cma

A finite element framework for continua with boundary energies. Part I: The two-dimensional case

A. Javili, P. Steinmann *

Lehrstuhl für Technische Mechanik, Universität Erlangen-Nürnberg, Egerlandstraße 5, D-91058 Erlangen, Germany

ARTICLE INFO

Article history:
Received 20 August 2008
Received in revised form 4 February 2009
Accepted 9 February 2009
Available online 20 February 2009

Keywords:
Boundary potentials
Surface tension

ABSTRACT

This contribution deals with the implications of boundary potential energies on the two-dimensional deformations of solids in the framework of the finite element method. Common modelling in continuum mechanics takes exclusively the bulk into account, nevertheless, neglecting possible contributions from the boundary. However, boundary effects sometimes play a dominant role in the material behavior, the most prominent example being surface tension. Within this contribution the boundary potentials are allowed, in general, to depend not only on the boundary deformation but also on the boundary deformation gradient and the spatial boundary tangent. For the finite element implementation, a suitable curvilinear convected coordinate system attached to the boundary is defined and corresponding geometrical and kinematical derivations completely based on a tensorial representation are carried out. Afterwards, the discretization of the generalized weak formulation, including boundary potentials, is performed and eventually numerical examples are presented to demonstrate the boundary effects due to different proposed material models.

1. Introduction

As it has been studied, e.g. [1,12,26,25] , surfaces of bodies and interfaces between pairs of bodies exhibit properties different from those associated with the bulk. This phenomenon is usually modelled in terms of surface tension. The notion of a scalar valued surface tension can be generalized to surface stress of tensorial nature, see, e.g. [3,33]. For a conservative case the surface stress derives from a boundary potential that depends on the surface deformation gradient similar to the case of elastic membranes/strings. Moreover, in material processing, the boundary of material is frequently exposed to, e.g. oxidation, ageing, grit blasting, plasma jet treatment, etc., thus obviously resulting in distinctively different properties in comparatively thin boundary layers. Likewise coating materials with thin films result clearly in different properties at the boundary. These effect could phenomenologically be modelled in terms of boundaries equipped with their own potential energy. In this manuscript the term surface is used rather than the interface, since we model a body with its surface attached to it. Of course both expressions can be used interchangeably in the context of the manuscript at hand. In the case pairs of bodies are considered, the term surface can be replaced by the term interface between the bodies.

From the physical point of view, it must be noted that a force term as the surface tension is a mechanical term, however, it is not the case for the energy term as the surface energy but since these two quantities have the same dimension, it has been the cause of confusion in literature. This fact is elaborated in detail in [37,5,6]. The term surface energy is usually accepted as an excess energy terms since a surface can be interpreted as a layer to which a certain energy is attached [37,24]. The surface energy can also be understood as a superficial energy term due to the rearrangement of atoms very near to a surface (see, e.g. [37,17]). Also, it is well accepted that on the surface of a liquid a certain surface stress in a spherically symmetric configuration acts. In the case of liquids, the value of the surface energy and surface stress are identical. This statement is proven and well explained in [37]. In this manuscript the scalar value of this spherically symmetric stress is referred to as surface tension which indeed is equal to the surface energy in case of liquids. From the theoretical point of view a substantial body of literature can be found on the surface tension and surface energy, see, e.g. [37,32,22,14,15] and references therein.

The numerical simulation of the surface of the body has been studied extensively when the bulk behaves like a fluid, e.g. [13,19,21,29] and also, with the variational formulation in [10,30,31]. A systematic treatment of the boundary surface and its coupling with the bulk based on potentials as implemented here was proposed in [38]. In this respect different behaviors for the surface of the continuum body can be considered by defining the respective surface potential energy and one does not have to stick to the surface tension as is customary for fluids. Therefore, the

* Corresponding author.
E-mail addresses: javili@ltm.uni-erlangen.de (A. Javili), paul.steinmann@ltm.uni-erlangen.de (P. Steinmann).

0045-7825/$ - see front matter © 2009 Elsevier B.V. All rights reserved.
doi:10.1016/j.cma.2009.02.008

surface of the body resembles a membrane coupled with the bulk. For the formulation of the membrane shell, see, e.g. [8] and references therein. Moreover, this approach opens up the possibility of having variational formulation based on energy minimization which can provide a suitable framework for mesh adaption, e.g. [34], and also capture singular problems such as wrinkling, e.g. [35]. In this contribution, in order to determine the behavior of the surface, different material models are proposed. The surface tension effect can result in numerical instabilities if the geometry of the problem is not properly chosen. In this case the classical methods to overcome the instabilities fail and therefore, a new methodology to get around this problem is proposed.

The suitable weak form of the pertinent balance equations and its discretized form are given. For the numerical implementation, a suitable curvilinear convected coordinate system attached to the surface of the body is defined and corresponding derivations completely based on a tensorial representation are carried out. The excellent efficiency of the numerical framework is shown by means of several examples.

2. Geometry and kinematics of boundaries

To set the stage, first some basic notations, terminologies and necessary results for the geometry of boundaries, i.e. curves in 2D, are briefly reviewed. More details can be found in the literature, e.g. [38,28,7].

A one-dimensional (smooth) curve $\mathscr{C}$ in the two-dimensional, embedding Euclidean space with coordinates $\boldsymbol{x}$ is parameterized by the arclength θ. Therefore,

$$\boldsymbol{x} = \boldsymbol{x}(\theta). \tag{1}$$

The corresponding tangent vector $\boldsymbol{t} \in T\mathscr{C}$ to the curve, together with the (principal) normal vector $\boldsymbol{m}$, orthogonal to $T\mathscr{C}$, are defined by

$$\boldsymbol{t} := \partial_\theta \boldsymbol{x} \quad \text{and} \quad \boldsymbol{m} := \partial_\theta \boldsymbol{t} / |\partial_\theta \boldsymbol{t}|. \tag{2}$$

Due to the parameterization of the curve in its arclength θ the tangent vector $\boldsymbol{t}$ has unit length and the curve line element $\mathrm{d}l$ is computed as

$$\mathrm{d}l = |\partial_\theta \boldsymbol{x}| \mathrm{d}\theta = |\boldsymbol{t}| \mathrm{d}\theta = \mathrm{d}\theta. \tag{3}$$

The Frénet–Serret formulae for the derivatives of the curve basis vectors reads

$$\partial_\theta \boldsymbol{t} = \mathrm{c}\boldsymbol{m} \quad \text{and} \quad \partial_\theta \boldsymbol{m} = -\mathrm{c}\boldsymbol{t}. \tag{4}$$

Here $\mathrm{c} = -\partial_\theta \boldsymbol{m} \cdot \boldsymbol{t} := -\widetilde{\mathrm{div}}\boldsymbol{m}$ denotes the scalar valued curvature of the curve.

Moreover, we define the (mixed-variant) curve second order unit tensor $\tilde{\boldsymbol{i}}$ as

$$\tilde{\boldsymbol{i}} := \boldsymbol{t} \otimes \boldsymbol{t} = \boldsymbol{i} - \boldsymbol{m} \otimes \boldsymbol{m}. \tag{5}$$

whereby $\boldsymbol{i}$ denotes the ordinary (mixed-variant) unit tensor. Clearly, the (mixed-variant) curve unit tensor acts as a curve (idempotent) projection tensor. The projection to the direction perpendicular to $\boldsymbol{t}$ is defined by the (mixed-variant) curve second order unit tensor $\tilde{\boldsymbol{i}}^\perp$ as

$$\tilde{\boldsymbol{i}}^\perp := \boldsymbol{i} - \tilde{\boldsymbol{i}}. \tag{6}$$

The projection to the direction perpendicular to the curve tangent is particularly important when anisotropic effects are considered.

Finally, the curve gradient and curve divergence operators for vector fields are defined by

$$\widetilde{\mathrm{Grad}}\{\bullet\} := \partial_\theta\{\bullet\} \otimes \boldsymbol{t} \quad \text{and} \quad \widetilde{\mathrm{div}}\{\bullet\} := \partial_\theta\{\bullet\} \cdot \boldsymbol{t}, \tag{7}$$

and as a consequence, one can observe that $\widetilde{\mathrm{Grad}}\{\bullet\} \cdot \boldsymbol{m} = \boldsymbol{0}$ holds by definition. For fields that are smooth in a two-dimensional neighborhood $\mathscr{N}$ of the curve, the curve gradient and curve divergence operators are alternatively defined as

$$\widetilde{\mathrm{Grad}}\{\bullet\} := \mathrm{Grad}\{\bullet\} \cdot \tilde{\boldsymbol{i}} \quad \text{and} \quad \widetilde{\mathrm{div}}\{\bullet\} := \widetilde{\mathrm{Grad}}\{\bullet\} : \tilde{\boldsymbol{i}}. \tag{8}$$

Curve Divergence Theorem. *Let $\mathscr{C}'$ denote a subcurve of $\mathscr{C}$. The outward normal to the boundary (end) points $\mathscr{P}' := \partial\mathscr{C}'$ of the subcurve $\mathscr{C}'$, living in the cotangent space to $\mathscr{C}'$, is denoted by $\tilde{\boldsymbol{m}}$. Then the curve divergence theorem for vector valued fields $\{\bullet\}$ reads*

$$\int_{\mathscr{C}'} \widetilde{\mathrm{div}}\{\bullet\}\,\mathrm{d}l = \sum_{\mathscr{P}'} \{\bullet\} \cdot \tilde{\boldsymbol{m}} - \int_{\mathscr{C}'} \mathrm{c}\{\bullet\} \cdot \boldsymbol{m}\,\mathrm{d}l. \tag{9}$$

The curve divergence theorem is the specialization of the ordinary Gauss theorem to curves. Especially if the vector field is tangent, i.e. $\{\bullet\} \cdot \boldsymbol{m} = 0$, the similarity is obvious.

Remark. Within the setting of continuum mechanics one can distinguish between curves $\mathscr{C}_0$ and $\mathscr{C}_t$ attached to the material and the spatial configuration $\mathscr{B}_0$ and $\mathscr{B}_t$ of a (deformable) continuum body. The above relations are notationally valid in the spatial configuration, for the same expressions in the material configuration, as a rule, all lower case letters are simply substituted by the corresponding upper case letters.

Consider next a continuum body that takes the material configuration $\mathscr{B}_0$ at time $t = 0$ and the spatial configuration $\mathscr{B}_t$ at time $t > 0$ as illustrated in Fig. 1. The material and spatial configuration are then identified with all the placements (coordinates in the three-dimensional, embedding Euclidean space) $\boldsymbol{X}$ and $\boldsymbol{x}$ that are occupied by the continuum body at time $t = 0$ and $t > 0$, respectively. The placement $\boldsymbol{x}$ and $\boldsymbol{X}$ in the spatial and the material configurations are related by the invertible (nonlinear) deformation map

$$\boldsymbol{x} = \boldsymbol{\varphi}(\boldsymbol{X}). \tag{10}$$

The associated deformation gradient or rather (invertible) linear tangent map between material and spatial line elements $\mathrm{d}\boldsymbol{x} \in T\mathscr{B}_t$ and $\mathrm{d}\boldsymbol{X} \in T\mathscr{B}_0$ is defined as

$$\boldsymbol{F} := \mathrm{Grad}\ \boldsymbol{\varphi}(\boldsymbol{X}). \tag{11}$$

Consequently, the associated (positive) Jacobian determinant or rather (invertible) linear volume map related to spatial and material volume elements $\mathrm{d}v$ and $\mathrm{d}V$, is defined as $J := \det \boldsymbol{F} > 0$.

The boundary of the continuum body is described or rather covered by a network of smooth one-dimensional curves in the

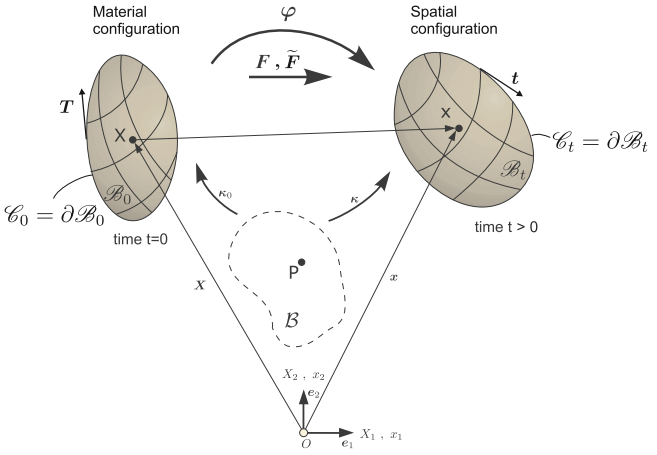

Fig. 1. Material and spatial configuration of a continuum body.

two-dimensional, embedding Euclidean space defined by the zero level sets $C^\kappa(\boldsymbol{X})=0$ of the level set functions $C^\kappa(\mathrm{X})$ for the material configuration with $\kappa=1,n_{\text{curv}}$. With these prescriptions at hand, e.g. the material configuration is defined by $\mathscr{B}_0:=\{\boldsymbol{X}|\ \cap C^\kappa(\boldsymbol{X})<0\}$ and then the network of boundary curves of, e.g. the material configuration is defined by $\mathscr{C}_0=\cup\mathscr{C}_0^\kappa:=\{\boldsymbol{X}|\ \cup C^\kappa(\boldsymbol{X})=0\}=\partial\mathscr{B}_0$. Finally, the n_{poin} intersections of the n_{curv} individual boundary curves define a set of boundary points $(\pi=1,n_{\text{poin}})$, e.g. of the material configuration $\mathscr{P}_0=\cup\mathscr{P}_0^\pi=\cap\mathscr{C}_0^\kappa$. Next as necessary preliminaries for the following developments, a number of relevant results pertaining exclusively to the kinematics of the boundary curves shall be assembled.

The curve deformation gradient $\widetilde{\boldsymbol{F}}$ or rather (non-invertible) linear curve tangent map between line elements $\mathrm{d}\boldsymbol{X}\in T\mathscr{C}_0$ and $\mathrm{d}\boldsymbol{x}\in T\mathscr{C}_t$ is defined as

$$\widetilde{\boldsymbol{F}}:=\widetilde{\mathrm{Grad}}\boldsymbol{\varphi}(\boldsymbol{X})=\lambda\boldsymbol{t}\otimes\boldsymbol{T}, \tag{12}$$

where $\lambda=\mathrm{d}l/\mathrm{d}L=\mathrm{d}\theta/\mathrm{d}\Theta$ denotes the curve stretch. Thus, boundary curve tangents $\boldsymbol{T}$ to $\mathscr{C}_0$ are convected by the deformation as

$$\boldsymbol{t}=\frac{\widetilde{\boldsymbol{F}}\cdot\boldsymbol{T}}{|\widetilde{\boldsymbol{F}}\cdot\boldsymbol{T}|}. \tag{13}$$

The curve deformation gradient $\widetilde{\boldsymbol{F}}=\boldsymbol{F}\cdot\widetilde{\boldsymbol{I}}$ is rank deficient and is thus not invertible. Nevertheless an inverse can be defined in the following generalized sense:

$$\widetilde{\boldsymbol{F}}^{-1}:=\Lambda\boldsymbol{T}\otimes\boldsymbol{t}, \tag{14}$$

where $\Lambda=\lambda^{-1}=\mathrm{d}L/\mathrm{d}l=\mathrm{d}\Theta/\mathrm{d}\theta$ denotes the inverse curve stretch and consequently

$$\widetilde{\boldsymbol{F}}\cdot\widetilde{\boldsymbol{F}}^{-1}=\lambda\Lambda[\boldsymbol{t}\otimes\boldsymbol{T}]\cdot[\boldsymbol{T}\otimes\boldsymbol{t}]=\tilde{\boldsymbol{i}}, \tag{15}$$

in which $\tilde{\boldsymbol{i}}$ denotes the curve unit tensor in the tangent space to the spatial configuration. We define curve line elements $\mathrm{d}L$ and $\mathrm{d}l$ of $\mathscr{C}_0$ and $\mathscr{C}_t$ to be mapped into each other by the curve Jacobian $\widetilde{J}$, i.e. $\mathrm{d}l=\widetilde{J}\,\mathrm{d}L$ with $\widetilde{J}:=\widetilde{\det}\widetilde{\boldsymbol{F}}$ where the curve determinant of the curve deformation gradient formally is defined as

$$\widetilde{\det}\widetilde{\boldsymbol{F}}:=\frac{|\widetilde{\boldsymbol{F}}\cdot\boldsymbol{T}|}{|\boldsymbol{T}|}. \tag{16}$$

Finally since $\lambda=\widetilde{J}$, for the two-dimensional case equations (12) and (14) lead to the simple result

$$\widetilde{\boldsymbol{F}}^{-T}=\frac{1}{\widetilde{J}^2}\widetilde{\boldsymbol{F}}. \tag{17}$$

3. Dirichlet principle of minimum potential energy

The bulk potential energy density U_0 per material unit volume in $\mathscr{B}_0$ is composed of internal and external contributions W_0 and V_0, respectively, as

$$U_0=W_0+V_0 \tag{18}$$

with

$$W_0=W_0(\boldsymbol{F};\boldsymbol{X})\quad\text{and}\quad V_0=V_0(\boldsymbol{\varphi};\boldsymbol{X}). \tag{19}$$

Likewise, the curve potential energy density u_0 per material unit length in $\mathscr{C}_0$ may consist of internal and external contributions w_0 and v_0, respectively, as

$$\mathrm{u}_0=\mathrm{w}_0+\mathrm{v}_0 \tag{20}$$

with

$$\mathrm{w}_0=\mathrm{w}_0(\widetilde{\boldsymbol{F}};\boldsymbol{X},\boldsymbol{T})\quad\text{and}\quad v_0=v_0(\boldsymbol{\varphi},\boldsymbol{t};\boldsymbol{X},\boldsymbol{T}). \tag{21}$$

Such constitutive laws can only be found from atomistic modelling. In the overview paper by Fischer et al. [37] and in the work by Haiss [20] some data on the constitutive law can be found. Moreover, a multiscale surface Helmholtz free energy can be constructed through the deployment of the surface Cauchy–Born hypothesis which is elaborated in [39].

In summary, the total potential energy functional $I=I(\boldsymbol{\varphi})$ that we seek to minimize with respect to all admissible variations $\delta\boldsymbol{\varphi}$ (spatial variations at fixed material placement) reads

$$I(\boldsymbol{\varphi}):=\int_{\mathscr{B}_0}U_0(\boldsymbol{\varphi},\boldsymbol{F};\boldsymbol{X})\,\mathrm{d}A+\int_{\mathscr{C}_0}\mathrm{u}_0(\boldsymbol{\varphi},\boldsymbol{t},\widetilde{\boldsymbol{F}};\boldsymbol{X},\boldsymbol{T})\,\mathrm{d}L. \tag{22}$$

Then the minimization of the total potential energy functional, $\delta I(\boldsymbol{\varphi})=0$, renders the principle of virtual work including contributions from boundary terms

$$\begin{aligned}&\int_{\mathscr{B}_0}\boldsymbol{P}:\mathrm{Grad}\delta\boldsymbol{\varphi}\,\mathrm{d}A+\int_{\mathscr{C}_0}\widetilde{\boldsymbol{P}}:\widetilde{\mathrm{Grad}}\delta\boldsymbol{\varphi}\,\mathrm{d}L+\int_{\mathscr{C}_0}[\tilde{\boldsymbol{\pi}}_t\otimes\boldsymbol{T}]:\widetilde{\mathrm{Grad}}\delta\boldsymbol{\varphi}\,\mathrm{d}L\\&\quad=\int_{\mathscr{B}_0}\boldsymbol{b}_0\cdot\delta\boldsymbol{\varphi}\,\mathrm{d}A+\int_{\mathscr{C}_0}\tilde{\boldsymbol{b}}_0\cdot\delta\boldsymbol{\varphi}\,\mathrm{d}L\quad\forall\delta\boldsymbol{\varphi}.\end{aligned} \tag{23}$$

The stress in two-point description and the distributed (volume) force related to the bulk $\mathscr{B}_0$ are defined, as usual, as

$$\boldsymbol{P}:=\partial_{\boldsymbol{F}}U_0\quad\text{and}\quad\boldsymbol{b}_0:=-\partial_{\boldsymbol{\varphi}}U_0. \tag{24}$$

Likewise, the stress in two-point description and the distributed force (the line load or rather tractions) related to the curves in $\mathscr{C}_0$ are defined as

$$\widetilde{\boldsymbol{P}}:=\partial_{\widetilde{\boldsymbol{F}}}\mathrm{u}_0\quad\text{and}\quad\tilde{\boldsymbol{b}}_0:=-\partial_{\boldsymbol{\varphi}}\mathrm{u}_0. \tag{25}$$

As an additional quantity a deformational curve shear related to $\mathscr{C}_0$ is defined as

$$\tilde{\boldsymbol{\pi}}_t:=\partial_{\boldsymbol{t}}\mathrm{u}_t\cdot\tilde{\boldsymbol{i}}^{\perp}, \tag{26}$$

where u_t denotes the curve internal potential energy density per spatial unit length. The denomination curve shear has been introduced before in [16], see also [38].

Moreover, with the help of identities

$$\begin{aligned}&\mathrm{Div}\boldsymbol{P}\cdot\delta\boldsymbol{\varphi}=\mathrm{Div}(\boldsymbol{P}^T\cdot\delta\boldsymbol{\varphi})-\boldsymbol{P}:\mathrm{Grad}\delta\boldsymbol{\varphi},\\&\widetilde{\mathrm{Div}}\widetilde{\boldsymbol{P}}\cdot\delta\boldsymbol{\varphi}=\widetilde{\mathrm{Div}}(\widetilde{\boldsymbol{P}}^T\cdot\delta\boldsymbol{\varphi})-\widetilde{\boldsymbol{P}}:\widetilde{\mathrm{Grad}}\delta\boldsymbol{\varphi},\\&\widetilde{\mathrm{Div}}(\tilde{\boldsymbol{\pi}}_t\otimes\boldsymbol{T})\cdot\delta\boldsymbol{\varphi}=\widetilde{\mathrm{Div}}([\boldsymbol{T}\otimes\tilde{\boldsymbol{\pi}}_t]\cdot\delta\boldsymbol{\varphi})-[\tilde{\boldsymbol{\pi}}_t\otimes\boldsymbol{T}]:\widetilde{\mathrm{Grad}}\delta\boldsymbol{\varphi},\end{aligned} \tag{27}$$

Eq. (23) transforms into

$$\begin{aligned}&\int_{\mathscr{B}_0}\mathrm{Div}\left(\boldsymbol{P}^T\cdot\delta\boldsymbol{\varphi}\right)\mathrm{d}A-\int_{\mathscr{B}_0}\mathrm{Div}\boldsymbol{P}\cdot\delta\boldsymbol{\varphi}\,\mathrm{d}A\\&\quad+\int_{\mathscr{C}_0}\widetilde{\mathrm{Div}}\left(\widetilde{\boldsymbol{P}}^T\cdot\delta\boldsymbol{\varphi}\right)\mathrm{d}L-\int_{\mathscr{C}_0}\widetilde{\mathrm{Div}}\widetilde{\boldsymbol{P}}\cdot\delta\boldsymbol{\varphi}\,\mathrm{d}L\\&\quad+\int_{\mathscr{C}_0}\widetilde{\mathrm{Div}}([\boldsymbol{T}\otimes\tilde{\boldsymbol{\pi}}_t]\cdot\delta\boldsymbol{\varphi})\,\mathrm{d}L-\int_{\mathscr{C}_0}\widetilde{\mathrm{Div}}(\tilde{\boldsymbol{\pi}}_t\otimes\boldsymbol{T})\cdot\delta\boldsymbol{\varphi}\,\mathrm{d}L\\&\quad=\int_{\mathscr{B}_0}\boldsymbol{b}_0\cdot\delta\boldsymbol{\varphi}\,\mathrm{d}A+\int_{\mathscr{C}_0}\tilde{\boldsymbol{b}}_0\cdot\delta\boldsymbol{\varphi}\,\mathrm{d}L\quad\forall\delta\boldsymbol{\varphi}.\end{aligned} \tag{28}$$

By applying the divergence theorem on the bulk and the boundary and considering the fact that $\boldsymbol{T}\cdot\boldsymbol{M}=0$, Eq. (28) is cast into

$$\begin{aligned}&-\int_{\mathscr{B}_0}\delta\boldsymbol{\varphi}\cdot\mathrm{Div}\boldsymbol{P}\,\mathrm{d}A-\int_{\mathscr{B}_0}\delta\boldsymbol{\varphi}\cdot\boldsymbol{b}_0\,\mathrm{d}A+\int_{\mathscr{C}_0}\delta\boldsymbol{\varphi}\cdot\boldsymbol{P}\cdot\boldsymbol{N}\,\mathrm{d}L\\&-\int_{\mathscr{C}_0}\delta\boldsymbol{\varphi}\cdot\widetilde{\mathrm{Div}}\left(\widetilde{\boldsymbol{P}}+\tilde{\boldsymbol{\pi}}_t\otimes\boldsymbol{T}\right)\mathrm{d}L-\int_{\mathscr{C}_0}\delta\boldsymbol{\varphi}\cdot\tilde{\boldsymbol{b}}_0\,\mathrm{d}L+\sum_{\mathscr{P}_0}\delta\boldsymbol{\varphi}\cdot\widetilde{\boldsymbol{P}}\cdot\boldsymbol{M}\\&=0\quad\forall\delta\boldsymbol{\varphi}\end{aligned} \tag{29}$$

and since the above expression holds for all spatial variations, it renders the equivalent local expressions:

$$\begin{cases} \mathrm{Div}\boldsymbol{P} + \boldsymbol{b}_0 = \boldsymbol{0} & \text{in } \mathscr{B}_0, \\ \boldsymbol{P}\cdot\boldsymbol{N} - \left[\widetilde{\mathrm{Div}}\left(\widetilde{\boldsymbol{P}} + \tilde{\boldsymbol{\pi}}_t \otimes \boldsymbol{T}\right) + \tilde{\boldsymbol{b}}_0\right] = \boldsymbol{0} & \text{on } \mathscr{C}_0, \\ \widetilde{\boldsymbol{P}}\cdot\boldsymbol{M} = \boldsymbol{0} & \text{at } \mathscr{P}_0, \end{cases} \tag{30}$$

which are the (localized) force balance in the bulk $\mathscr{B}_0$, the (localized) force balance or Neumann-type boundary condition on the boundary curves in $\mathscr{C}_0 = \partial\mathscr{B}_0$ and the (localized) force balance at points $\mathscr{P}_0$, respectively. We keep in mind that the (localized) force balance at points relies on the fact that the curve is smooth and it does not hold true for the sharp kinks. More details on this is given in [38]. Note that we recover for the special case $\mathrm{u}_0 = \mathrm{u}_0(\boldsymbol{\varphi})$ the ordinary traction equilibrium condition $\boldsymbol{P}\cdot\boldsymbol{N} = \tilde{\boldsymbol{b}}_0$.

It is noteworthy that $\boldsymbol{N}$ denotes the outward normal vector to the boundary in material configuration, however, $\boldsymbol{M}$ is the normal vector to the curve pointing to the center of the curvature. Therefore, depending on the sign of the curvature $\boldsymbol{N} = \pm\boldsymbol{M}$. However, the sign does not matter for $\boldsymbol{M}\otimes\boldsymbol{M}$.

4. Finite element discretization and implementation

In order to have an efficient finite element framework, the curve elements have to be consistent with the bulk. For instance, if the bulk is discretized by means of quadratic triangles, the curve elements are also quadratic. From the point of view of implementation, this choice has the advantage that the edges of the bulk element can be regarded as curve elements if they only belong to one bulk element. This fact is illustrated in Fig. 2 for quadratic triangles.

The principle of virtual work achieved in (23) is discretized, as alluded in Fig. 3, into a set of bulk elements and a set of curve elements with

$$\mathscr{B}_0 = \bigcup_{\beta=1}^{n_{\text{b-el}}} \mathscr{B}_0^{\beta} \qquad \mathscr{C}_0 = \bigcup_{\gamma=1}^{n_{\text{c-el}}} \mathscr{C}_0^{\gamma}, \tag{31}$$

where $n_{\text{b-el}}$ stands for the number of bulk elements and $n_{\text{c-el}}$ stands for the number of curve elements.[1]

The geometry for each curve element can be written as a function of natural coordinate ξ, defined in the Fig. 4, by using standard interpolations and Galerkin approximations

$$\boldsymbol{\varphi}(\xi) \approx \sum_{i=1}^{N_{\text{node}}} \widetilde{N}^i(\xi)\boldsymbol{\varphi}^i \quad \text{and} \quad \boldsymbol{X}(\xi) \approx \sum_{i=1}^{N_{\text{node}}} \widetilde{N}^i(\xi)\boldsymbol{X}^i. \tag{32}$$

Here $\xi \in [0,1]$ is the natural coordinate in one dimension and $\widetilde{N}^i$ is the standard shape function of the curve element at node i. This convention for the superscript i holds for the whole work. In order to distinguish between the shape functions for the bulk and the shape functions for the curve element, $\widetilde{N}$ is used. Furthermore, the curve deformation gradient results in

$$\widetilde{\boldsymbol{F}} = \widetilde{\mathrm{Grad}}\boldsymbol{\varphi} \approx \sum_{i=1}^{N_{\text{node}}} \boldsymbol{\varphi}^i \otimes \widetilde{\mathrm{Grad}}\widetilde{N}^i, \tag{33}$$

where

$$\begin{aligned} \widetilde{\mathrm{Grad}}\widetilde{N}^i &= \partial_\Theta \widetilde{N}^i\, \boldsymbol{T} = \frac{\partial\xi}{\partial\Theta}\, \partial_\xi \widetilde{N}^i\, \boldsymbol{T} = \left[\frac{\partial\Theta}{\partial\xi}\right]^{-1} \partial_\xi \widetilde{N}^i\, \boldsymbol{T} \\ &= |\partial_\xi \boldsymbol{X}|^{-1}\, \partial_\xi \widetilde{N}^i\, \boldsymbol{T}. \end{aligned} \tag{34}$$

[1] The discretization procedure for the bulk is skipped, for the sake of space. Nevertheless, a similar strategy can be used as has been introduced in the literature, e.g. [11,36].

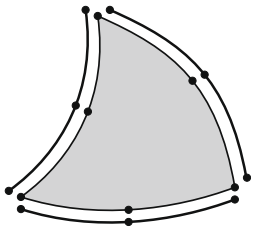

Fig. 2. Illustration of consistency of the curve elements with the bulk.

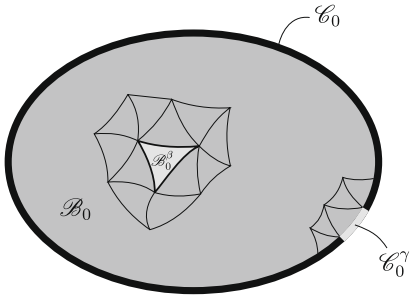

Fig. 3. Discretization of the bulk and the boundary.

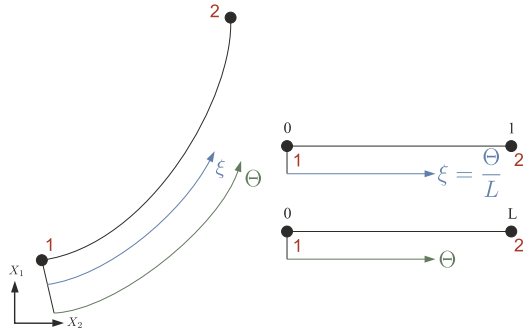

Fig. 4. Curvilinear coordinate system assigned to the one-dimensional curve element.

The unit tangent in the reference configuration, can be computed by

$$\boldsymbol{T} = \frac{\partial_\xi \boldsymbol{X}}{|\partial_\xi \boldsymbol{X}|}. \tag{35}$$

Equipped with all the above formulae, the weak form of the balance equation associated with bulk element β with attached curve elements γ for the node i is eventually discretized into

$$\begin{aligned} &\int_{\mathscr{B}_0^{\beta}} \boldsymbol{P}\cdot\mathrm{Grad}N^i\,\mathrm{d}A + \int_{\mathscr{C}_0^{\gamma}} \widetilde{\boldsymbol{P}}\cdot\widetilde{\mathrm{Grad}}\widetilde{N}^i\,\mathrm{d}L + \int_{\mathscr{C}_0^{\gamma}} [\tilde{\boldsymbol{\pi}}_t\otimes\boldsymbol{T}]\cdot\widetilde{\mathrm{Grad}}\widetilde{N}^i\,\mathrm{d}L \\ &\quad = \int_{\mathscr{B}_0^{\beta}} \boldsymbol{b}_0 N^i\,\mathrm{d}A + \int_{\mathscr{C}_0^{\gamma}} \tilde{\boldsymbol{b}}_0\widetilde{N}^i\,\mathrm{d}L. \end{aligned} \tag{36}$$

In order to solve (36), the Newton–Raphson scheme can be utilized. For that, first the residual vector for each local node i associated with the bulk element β with attached curve elements γ, is defined as

$$\begin{aligned} \boldsymbol{R}_e^i &:= \int_{\mathscr{B}_0^{\beta}} \boldsymbol{P}\cdot\mathrm{Grad}N^i\,\mathrm{d}A + \int_{\mathscr{C}_0^{\gamma}} \left[\widetilde{\boldsymbol{P}} + \tilde{\boldsymbol{\pi}}_t\otimes\boldsymbol{T}\right]\cdot\widetilde{\mathrm{Grad}}\widetilde{N}^i\,\mathrm{d}L \\ &\quad - \int_{\mathscr{B}_0^{\beta}} \boldsymbol{b}_0 N^i\,\mathrm{d}A - \int_{\mathscr{C}_0^{\gamma}} \tilde{\boldsymbol{b}}_0\widetilde{N}^i\,\mathrm{d}L. \end{aligned} \tag{37}$$

It must be emphasized that (37) takes both contributions from the bulk and the boundary into account, however, if we consider an element whose edges are not the boundaries of the continuum body,

the first term integrating over the boundaries will identically vanish since it is only meaningful in the presence of the boundaries.

The global residual at the global node J is defined by

$$\boldsymbol{R}^J := \mathop{\mathsf{A}}_{e=1}^{n_{\mathrm{el}}} \boldsymbol{R}_e^j, \tag{38}$$

where the corresponding local node number in an element or curve element e to the global node number J is denoted by $j = 1, n_{\mathrm{ne}}$ and n_{ne} is the number of nodes per element or curve element. Herein the operator $\mathop{\mathsf{A}}_{e=1}^{n_{\mathrm{el}}}$ denotes the assembly of all element and curve elements contributions at the global node $J = 1, n_{\mathrm{np}}$ where n_{np} is the total number of nodes.

The consistent linearization of the resulting system of equations, would be

$$\boldsymbol{R}(\boldsymbol{d}) + \left.\frac{\partial \boldsymbol{R}}{\partial \boldsymbol{d}}\right|_n \Delta \boldsymbol{d} = \boldsymbol{0} \quad \text{and} \quad \boldsymbol{d}_{n+1} = \boldsymbol{d}_n + \Delta \boldsymbol{d}, \tag{39}$$

in which n stands for the iteration step and $\boldsymbol{R}$ and $\boldsymbol{d}$ are the global vectors of residual and spatial coordinates defined, e.g. by

$$\begin{aligned} \boldsymbol{d} &= [\boldsymbol{\varphi}^1, \boldsymbol{\varphi}^2, \ldots, \boldsymbol{\varphi}^J, \ldots, \boldsymbol{\varphi}^{n_{\mathrm{np}}}]^T, \\ \boldsymbol{R} &= [\boldsymbol{R}^1, \boldsymbol{R}^2, \ldots, \boldsymbol{R}^J, \ldots, \boldsymbol{R}^{n_{\mathrm{np}}}]^T. \end{aligned} \tag{40}$$

Solving (39) results in the spatial coordinate increment, $\Delta \boldsymbol{d}$ and consequently $\boldsymbol{d}_{n+1}$.

The local tangent stiffness would be

$$\begin{aligned} \left[\boldsymbol{K}_e^{ij}\right]_{ac} &= \left[\frac{\partial \boldsymbol{R}_e^i}{\partial \boldsymbol{\varphi}^j}\right]_{ac} \\ &= \int_{\mathscr{B}_0^\beta} \left\{\mathrm{Grad} N^i\right\}_b \{\mathbb{A}\}_{abcd} \left\{\mathrm{Grad} N^j\right\}_d \mathrm{d}A \\ &\quad + \int_{\mathscr{C}_0^\gamma} \left\{\widetilde{\mathrm{Grad}}\, \widetilde{N}^i\right\}_b \{\widetilde{\mathbb{A}}\}_{abcd} \left\{\widetilde{\mathrm{Grad}}\, \widetilde{N}^j\right\}_d \mathrm{d}L \\ &\quad + \int_{\mathscr{C}_0^\gamma} \left\{\widetilde{\mathrm{Grad}}\, \widetilde{N}^i\right\}_b \{\widetilde{\mathbb{H}}\}_{abcd} \left\{\widetilde{\mathrm{Grad}}\, \widetilde{N}^j\right\}_d \mathrm{d}L, \end{aligned} \tag{41}$$

in which $\mathbb{A}$ is the fourth order elasticity two-point tensor as has been introduced in [9]. $\widetilde{\mathbb{A}}$ and $\widetilde{\mathbb{H}}$ are defined, in analogy, as follows:

$$\mathbb{A} = \frac{\partial \boldsymbol{P}}{\partial \boldsymbol{F}} \quad \text{and} \quad \widetilde{\mathbb{A}} = \frac{\partial \widetilde{\boldsymbol{P}}}{\partial \widetilde{\boldsymbol{F}}} \quad \text{and} \quad \widetilde{\mathbb{H}} = \frac{\partial [\tilde{\boldsymbol{\pi}}_t \otimes \boldsymbol{T}]}{\partial \widetilde{\boldsymbol{F}}}. \tag{42}$$

Finally in analogy to (38), the global tangent stiffness of the whole system has to be assembled

$$\boldsymbol{K}^{IJ} = \mathop{\mathsf{A}}_{e=1}^{n_{\mathrm{el}}} \boldsymbol{K}_e^{ij}. \tag{43}$$

It is noteworthy that the assembly operator introduced here is slightly different from that introduced in the literature, e.g. [18,27], in the sense that here the contributions from both the bulk and the boundary curve have to be taken into account.

5. Examples for boundary potentials

In order to model a specific material behavior of the boundary, first the internal potential energy of the boundary material, $\mathrm{w}_0(\widetilde{\boldsymbol{F}}; \boldsymbol{X}, \boldsymbol{T})$, is defined. Next, the corresponding derivations are carried out so as to achieve the boundary Piola stress and elasticity tensor $\widetilde{\boldsymbol{P}}$ and $\widetilde{\mathbb{A}}$, respectively, as well as $\tilde{\boldsymbol{\pi}}_t$ and $\widetilde{\mathbb{H}}$ which are contributions explicitly from the anisotropic part of the boundary energy. In this contribution two elementary options are proposed for isotropic boundary potentials in Sections 5.1 and 5.2, respectively. The first option models boundaries which behave like a neo-Hookean material and the second one models the typical surface tension. In Section 5.3 a combination of these two models is investigated which enables us to capture a variety of isotropic surface material behaviors. Afterwards, in Section 5.4 an anisotropic model for surface energy is proposed.

5.1. Neo-Hookean type boundary potential

For a boundary material which behaves analogously to a neo-Hookean material, however in one dimension, so that it mimics the format, e.g. advocated in [23], the internal potential energy can be expressed as

$$\mathrm{w}_0(\widetilde{\boldsymbol{F}}) = \frac{1}{2}\tilde{\mu}\left[\widetilde{\boldsymbol{F}} : \widetilde{\boldsymbol{F}} - 1 - 2\log \widetilde{J}\right]. \tag{44}$$

By the help of (12),

$$\widetilde{\boldsymbol{F}} : \widetilde{\boldsymbol{F}} = [\lambda \boldsymbol{t} \otimes \boldsymbol{T}] : [\lambda \boldsymbol{t} \otimes \boldsymbol{T}] = \lambda^2 = \widetilde{J}^2, \tag{45}$$

Eq. (44) might be simplified into

$$\mathrm{w}_0(\widetilde{\boldsymbol{F}}) = \frac{1}{2}\tilde{\mu}\left[\widetilde{J}^2 - 1 - 2\log \widetilde{J}\right]. \tag{46}$$

The material model proposed here tends to keep the length of the curve elements equal to the reference length, i.e. $\lambda \doteq 1$. The corresponding boundary Piola stress tensor takes the following explicit expression:

$$\widetilde{\boldsymbol{P}} = \frac{\partial \mathrm{w}_0}{\partial \widetilde{\boldsymbol{F}}} = \frac{\tilde{\mu}}{\widetilde{J}^2}[\widetilde{J}^2 - 1]\widetilde{\boldsymbol{F}}. \tag{47}$$

Moreover, the explicit representations for the fourth order elasticity tensor $\widetilde{\mathbb{A}}$ will be

$$\widetilde{\mathbb{A}} = \frac{\partial \widetilde{\boldsymbol{P}}}{\partial \widetilde{\boldsymbol{F}}} = \frac{2\tilde{\mu}}{\widetilde{J}^4}\widetilde{\boldsymbol{F}} \otimes \widetilde{\boldsymbol{F}} + \frac{\tilde{\mu}}{\widetilde{J}^2}[\widetilde{J}^2 - 1]\widetilde{\mathbb{I}} \tag{48}$$

in which

$$\widetilde{\mathbb{I}} = \boldsymbol{I} \overline{\otimes} \widetilde{\boldsymbol{I}} \quad \text{with } \{\boldsymbol{A} \overline{\otimes} \boldsymbol{B}\}_{ijkl} = A_{ik}\, B_{jl}. \tag{49}$$

5.2. Surface tension boundary potential

The second material model for the boundary captures the surface effects in fluids, i.e. surface tension; more details can be found in [4]. For this model the potential energy per unit deformed area has to be constant due to constant surface tension on the whole boundary, see, e.g. [2]. Therefore

$$\mathrm{w}_t = \mathrm{const.} = \widetilde{\lambda} \tag{50}$$

and correspondingly

$$\mathrm{w}_0(\widetilde{\boldsymbol{F}}) = \widetilde{\lambda}\widetilde{J}. \tag{51}$$

The associated boundary Piola stress tensor takes the following explicit expression:

$$\widetilde{\boldsymbol{P}} = \frac{\partial \mathrm{w}_0}{\partial \widetilde{\boldsymbol{F}}} = \frac{\widetilde{\lambda}}{\widetilde{J}}\widetilde{\boldsymbol{F}}. \tag{52}$$

Note that the push-forward of the boundary Piola stress tensor results in the boundary Cauchy stress tensor, i.e.

$$\widetilde{\boldsymbol{\sigma}} = \frac{1}{\widetilde{J}}\,\widetilde{\boldsymbol{P}}\,\widetilde{\boldsymbol{F}}^T = \frac{1}{\widetilde{J}}\,\frac{\widetilde{\lambda}}{\widetilde{J}}\,\widetilde{\boldsymbol{F}} \cdot \widetilde{\boldsymbol{F}}^T = \widetilde{\lambda}\,\widetilde{\boldsymbol{I}} \tag{53}$$

in which the identity $\widetilde{\boldsymbol{F}} \cdot \widetilde{\boldsymbol{F}}^T = \widetilde{J}^2\,\widetilde{\boldsymbol{I}}$ has been deployed. Eq. (53) is remarkable since it proves that the scalar value of the spherically symmetric surface Cauchy stress, is equal to the surface energy per unit deformed area in the current configuration, here $\widetilde{\lambda}$. In other words, in case of liquids the surface energy is identical to surface stress. This duality has caused a lot of confusion in the literature.

Nevertheless, in this manuscript this boundary potential is named surface tension boundary potential and must not be confused with surface stress in general.

Moreover, the explicit representations for the fourth order elasticity tensor $\widetilde{\mathbb{A}}$ will be

$$\widetilde{\mathbb{A}} = \frac{\partial \widetilde{\boldsymbol{P}}}{\partial \widetilde{\boldsymbol{F}}} = \frac{\widetilde{\lambda}}{\widetilde{J}}\left[\widetilde{\mathbb{I}} - \frac{1}{\widetilde{J}^2}\widetilde{\boldsymbol{F}} \otimes \widetilde{\boldsymbol{F}}\right]. \tag{54}$$

Remark. For the surface tension model one has to notice that the energy of the surface, in general, will not be minimum in the reference configuration, i.e. this model does not satisfy the growth conditions. Thus, this model has a rather unique characteristic as compared to most of the material models and hence it requires more investigations. Moreover, it always tends to shrink the surface area and to result in a constant curvature on the surface. Consequently, this type of boundary model tends to transfer any material curve to a point and only the resistance from the bulk will lead to an equilibrium state other than that. In other words, if the prescribed geometry of the problem does not coincide with that of the equilibrium state, the surface tension effect acts analogous to external loads on the surface. This shows that the surface tension effect, can result in computational instabilities and accordingly the solution may not be achieved. It must also be noted that in this case the classical strategies to overcome the instabilities fail and the reason lies in the fact that most of the methodologies proposed in the literature are improving either the finite elements or the loading method, however, in this case neither the finite element nor the loading is the source of the instabilities. In order to get around this problem, one has to apply the surface tension incrementally even though it is a material parameter. This innovative approach provides a very robust algorithm in the proposed finite element framework and the excellent efficiency of that is illustrated by means of several examples.

5.3. Combined boundary potential

The material model proposed in Section 5.2 tries to satisfy a constant curvature condition over the boundary and moreover, to minimize the length as much as possible. The material model proposed in Section 5.1 tends to keep the length of the curve elements equal to the reference length. These two facts motivate us to propose the third material model which is a combination of the two proposed models which enables us to capture a variety of different surface material behaviors. After some mathematical manipulations the combined boundary potential follows as:

$$\mathrm{w}_0(\widetilde{\boldsymbol{F}}) = \widetilde{\lambda}\widetilde{J} + \frac{1}{2}\tilde{\mu}\left[\widetilde{\boldsymbol{F}} : \widetilde{\boldsymbol{F}} - 1 - 2\log\widetilde{J}\right]. \tag{55}$$

The corresponding boundary Piola stress tensor takes the explicit expression

$$\widetilde{\boldsymbol{P}} = \frac{\partial \mathrm{w}_0}{\partial \widetilde{\boldsymbol{F}}} = \left[\frac{\widetilde{\lambda}}{\widetilde{J}} + \frac{\tilde{\mu}}{\widetilde{J}^2}[\widetilde{J}^2 - 1]\right]\widetilde{\boldsymbol{F}}. \tag{56}$$

Moreover, the explicit representations for the fourth order elasticity tensor, $\widetilde{\mathbb{A}}$ will be

$$\widetilde{\mathbb{A}} = \frac{\partial \widetilde{\boldsymbol{P}}}{\partial \widetilde{\boldsymbol{F}}} = \frac{1}{\widetilde{J}^4}\left[2\tilde{\mu} - \widetilde{J}\widetilde{\lambda}\right]\widetilde{\boldsymbol{F}} \otimes \widetilde{\boldsymbol{F}} + \frac{1}{\widetilde{J}^2}\left[\widetilde{J}\widetilde{\lambda} + \tilde{\mu}[\widetilde{J}^2 - 1]\right]\widetilde{\mathbb{I}}. \tag{57}$$

5.4. Anisotropic surface tension boundary potential

The proposed anisotropic material model for the boundary captures the anisotropic surface tension. This model represents the surface tension effect but depends on the curve stretch and the curve tangent instead of being constant all over the surface. For this model the potential energy per unit deformed area consists of a constant $\widetilde{\lambda}$ due to constant surface tension on the whole boundary plus an additional part as a function of the curve tangent $\boldsymbol{t}$ and the curve stretch $\widetilde{J}$. The material parameter $\widetilde{\alpha}$ is chosen in order to control the anisotropic contribution compared to the isotropic part. The vector $\boldsymbol{e}$ is a given unit vector characterizing a distinguished direction. Therefore

$$\mathrm{w}_t = \widetilde{\lambda}\left[1 + \widetilde{\alpha}\,\widetilde{J}[\boldsymbol{t}\cdot\boldsymbol{e}]^2\right], \tag{58}$$

and consequently,

$$\mathrm{w}_0 = \widetilde{\lambda}\widetilde{J} + \widetilde{\alpha}\widetilde{\lambda}[\widetilde{\boldsymbol{F}} : \widetilde{\boldsymbol{\Gamma}}]^2, \tag{59}$$

where $\widetilde{\boldsymbol{\Gamma}} := \boldsymbol{e} \otimes \boldsymbol{T}$. The corresponding boundary Piola stress tensor takes the explicit expression

$$\widetilde{\boldsymbol{P}} = \frac{\partial \mathrm{w}_0}{\partial \widetilde{\boldsymbol{F}}} = \frac{\widetilde{\lambda}}{\widetilde{J}}\widetilde{\boldsymbol{F}} + 2\widetilde{\alpha}\widetilde{\lambda}[\widetilde{\boldsymbol{F}} : \widetilde{\boldsymbol{\Gamma}}]\widetilde{\boldsymbol{\Gamma}}. \tag{60}$$

Moreover, the explicit representations for the fourth order elasticity tensor, $\widetilde{\mathbb{A}}$ will be

$$\widetilde{\mathbb{A}} = \frac{\partial \widetilde{\boldsymbol{P}}}{\partial \widetilde{\boldsymbol{F}}} = \frac{\widetilde{\lambda}}{\widetilde{J}}\left[\widetilde{\mathbb{I}} - \frac{1}{\widetilde{J}^2}\widetilde{\boldsymbol{F}} \otimes \widetilde{\boldsymbol{F}}\right] + 2\widetilde{\alpha}\widetilde{\lambda}\ \widetilde{\boldsymbol{\Gamma}} \otimes \widetilde{\boldsymbol{\Gamma}}. \tag{61}$$

The deformational curve shear $\tilde{\boldsymbol{\pi}}_t$ can be derived as

$$\tilde{\boldsymbol{\pi}}_t = \partial_{\boldsymbol{t}}\mathrm{w}_t \cdot \tilde{\boldsymbol{i}}^{\perp} = 2\widetilde{\lambda}\widetilde{\alpha}\widetilde{J}[\boldsymbol{t}\cdot\boldsymbol{e}]\tilde{\boldsymbol{e}}^{\perp}. \tag{62}$$

Finally,

$$\widetilde{\mathbb{H}} = \frac{\partial[\tilde{\boldsymbol{\pi}}_t \otimes \boldsymbol{T}]}{\partial \widetilde{\boldsymbol{F}}} = \widetilde{A}\,\underline{\boldsymbol{\emptyset}}\,\boldsymbol{T}, \tag{63}$$

in which the non-standard tensor operator $\underline{\boldsymbol{\emptyset}}$ is defined by

$$\{A\,\underline{\boldsymbol{\emptyset}}\,\boldsymbol{v}\}_{ijkl} = A_{ikl}\ v_j \tag{64}$$

and the third order tensor $\widetilde{A}$ is

$$\widetilde{A} = \frac{\partial \tilde{\boldsymbol{\pi}}_t}{\partial \widetilde{\boldsymbol{F}}}. \tag{65}$$

6. Numerical examples

A number of examples in order to illustrate the effects of boundary potentials are elaborated here. For all the examples the neo-Hookean material model is assumed for the bulk with given Lamé parameters, $\bar{\lambda}$ and $\bar{\mu}$, as

$$W_0(\boldsymbol{F};\boldsymbol{X}) = \frac{1}{2}\bar{\lambda}\log^2 J + \frac{1}{2}\bar{\mu}[\boldsymbol{F} : \boldsymbol{F} - 2 - 2\log J], \quad J = \det\boldsymbol{F}. \tag{66}$$

Therefore,

$$\boldsymbol{P} = \frac{\partial W_0}{\partial \boldsymbol{F}} = [\bar{\lambda}\log J - \bar{\mu}]\boldsymbol{F}^{-T} + \bar{\mu}\boldsymbol{F} \tag{67}$$

and

$$\mathbb{A} = \frac{\partial \boldsymbol{P}}{\partial \boldsymbol{F}} = \bar{\lambda}\ \boldsymbol{F}^{-T} \otimes \boldsymbol{F}^{-T} + \bar{\mu}\ \mathbf{1}\overline{\otimes}\mathbf{1} + [\bar{\mu} - \bar{\lambda}\log J]\boldsymbol{F}^{-T}\underline{\otimes}\boldsymbol{F}^{-1}, \tag{68}$$

where

$$\{\boldsymbol{A}\underline{\otimes}\boldsymbol{B}\}_{ijkl} = A_{il}\ B_{jk}. \tag{69}$$

For the examples 6.1–6.5 the combined material model proposed in Section 5.3 is used for the boundary and for the examples 6.6 and 6.7 the anisotropic model proposed in Section 5.4 is deployed.

The bulk is discretized by means of six-noded triangle elements for the examples 6.1–6.5 and by means of nine-noded quadrangle

elements for the examples 6.6–6.7. Consistent with the bulk for the surface the three-noded one-dimensional element is used.

6.1. First illustration of neo-Hookean type boundary effects

In this example a square with hole, under prescribed displacements at end edges, is assumed as shown in Fig. 5. For the boundary the material parameter $\widetilde{\lambda} = 0$ is assumed. For the bulk, the Lamé parameters are assumed to be $\bar{\mu} = 10$ and $\bar{\lambda} = 10$. The effects of the boundary for different values of $\tilde{\mu}$ is illustrated in Fig. 5.

In order to analyze the effect of the material parameter $\tilde{\mu}$ and to show how it will resist against changing the length of the boundary curves, the ratio of the summation of the current curve elements lengths over the summation of the reference lengths $\widetilde{J}_{\text{avg}}$ versus

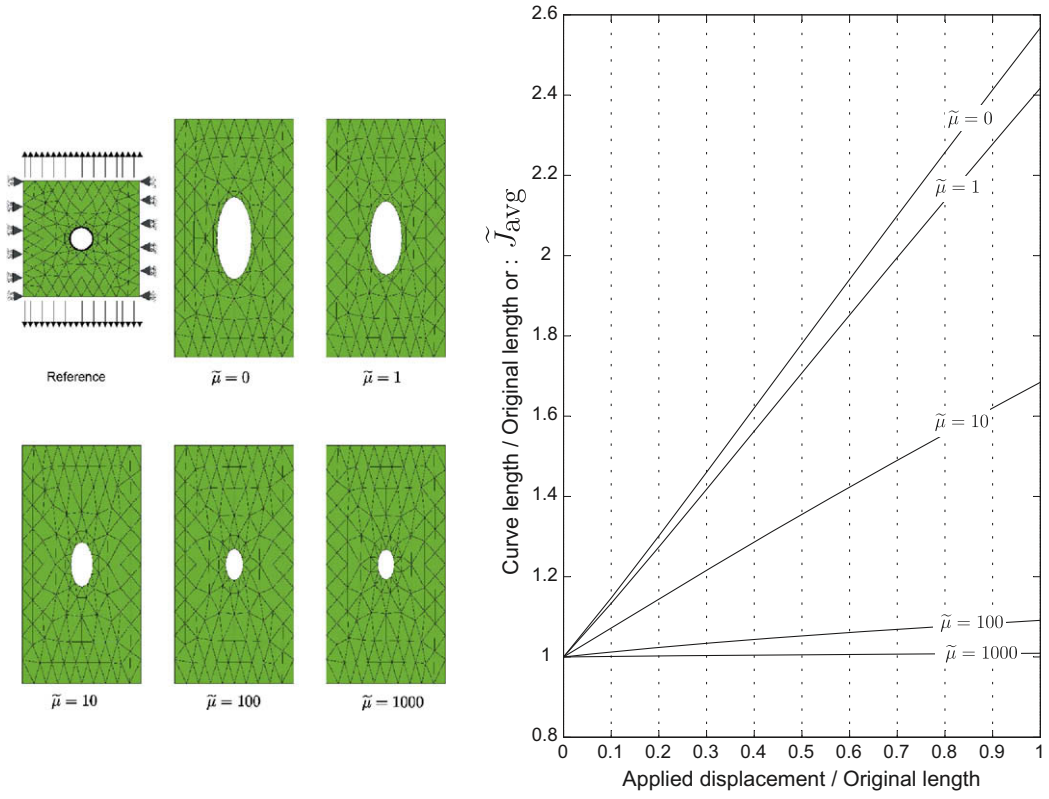

Fig. 5. Boundary effects with $\bar{\lambda} = 0$.

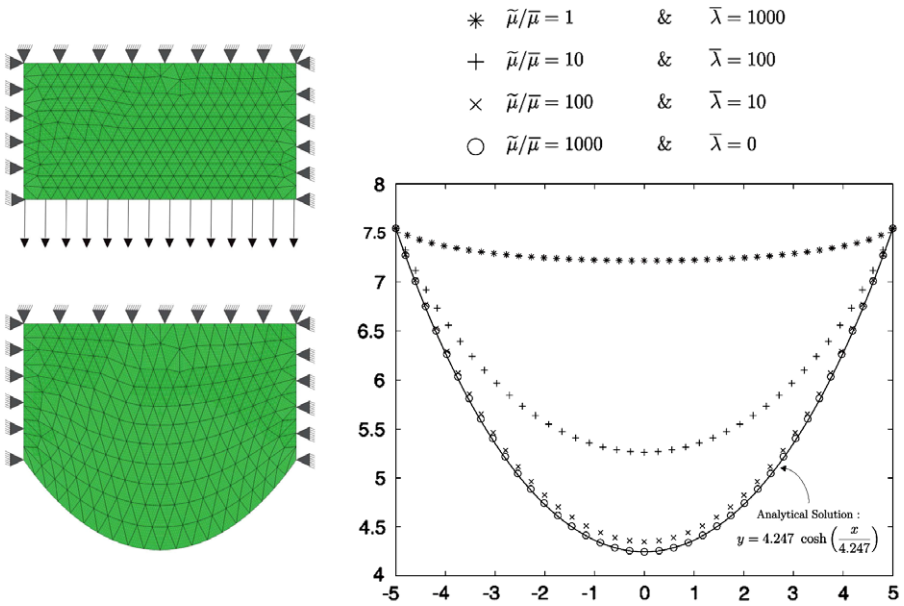

Fig. 6. A model to illustrate the hanging rope.

normalized applied displacement is shown in Fig. 5 (right). As is expected, in the limiting case, for $\bar{\mu} \to \infty$ the length of the boundary curve will remain constant.

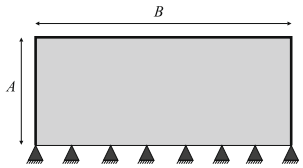

Fig. 7. A model rectangle to show surface effects.

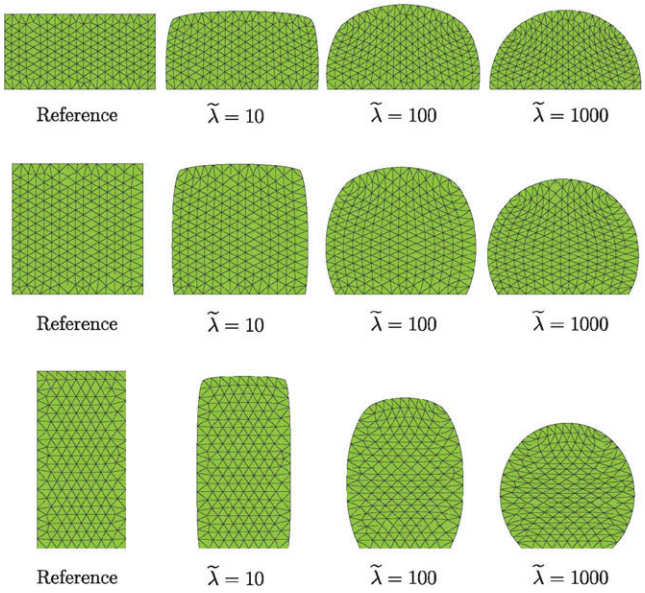

Fig. 8. Boundary effects with $\bar{\mu} = 0$.

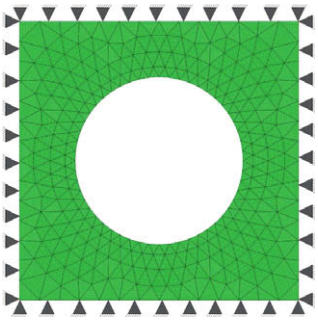

Fig. 9. A model square with hole in it to show surface effects.

6.2. Second illustration of neo-Hookean type boundary effects

For the next example, a rectangular block, as shown in Fig. 6, is considered which is fixed at three edges and on the free edge at the bottom a constant distributed load is applied. On the boundary curves the material parameter $\widetilde{\lambda} = 0$ is assumed, therefore the boundary curve shows only the neo-Hookean type material behavior. The width of the rectangle is 10 and the height is 5. This example is solved for four different sets of material parameters and the corresponding results are shown in the Fig. 6 (right). One can see that in the absence of the bulk, that is $\bar{\mu}/\bar{\mu} \to \infty$ and $\bar{\lambda} = 0$, the shape of the boundary curve approaches that of the hanging rope under its self weight. This example shows an excellent consistency with theory and represents the efficiency of the proposed method. The external load is applied incrementally and the typical convergence behavior, the norm of the residual, is quadratic and the convergence behavior of two arbitrary steps are as follows:

```
Convergence Behavior of Step 9:
        3.316625e−02    4.338180e−03    1.376239e−05
4.984942e−10
Convergence Behavior of Step 13:
        3.316625e−02    1.979847e−03    2.329720e−06
8.547254e−12
```

6.3. First illustration of surface tension type boundary effects

In this example a rectangle, as shown in Fig. 7, is considered with different aspect ratios of $A/B = 1/2, A/B = 1$ and $A/B = 2$. To that end, the width of the element $B = 10$ is fixed and A varies. The lower edge of the rectangle is fixed and for the whole boundary the material parameter $\bar{\mu} = 0$ is assumed. For the bulk, the Lamé parameters are assumed to be $\bar{\mu} = 10$ and $\bar{\lambda} = 1000$. The effects of the boundary for different values of $\widetilde{\lambda}$ is illustrated in Fig. 8.

6.4. Second illustration of surface tension type boundary effects

For the next example a square with a hole as shown in Fig. 9 is considered. Again in order to limit the surface effects to the contributions coming from surface tension model the material parameter $\bar{\mu} = 0$ is assumed. Furthermore, for the bulk the Lamé parameters are assumed to be $\bar{\mu} = 10$ and $\bar{\lambda} = 100$. The effects of the boundary potential for different values of $\widetilde{\lambda}$ is illustrated in Fig. 10.

6.5. Third illustration of surface tension type boundary effects

In this example a rectangle, as shown in Fig. 11, is considered with different aspect ratios of $A/B = 1/2, A/B = 1$ and $A/B = 2$ and the area of the bulk is fixed such that for the first row $B = 10$ and $A = 5$ and for the last one $B = 5$ and $A = 10$ is assumed. The lower edge of the model rectangle is fixed only at the

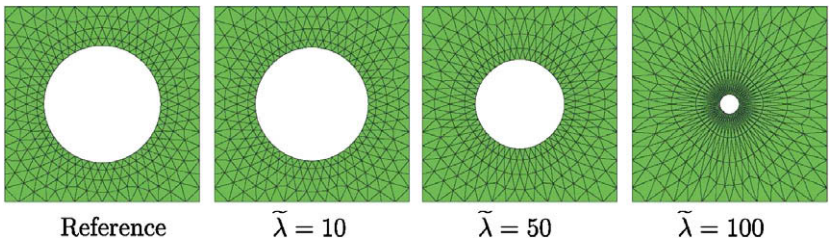

Fig. 10. Boundary effects with $\bar{\mu} = 0$.

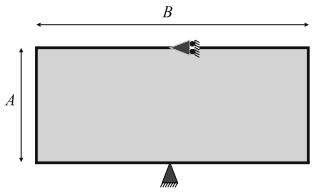

Fig. 11. A model rectangle to show surface effects.

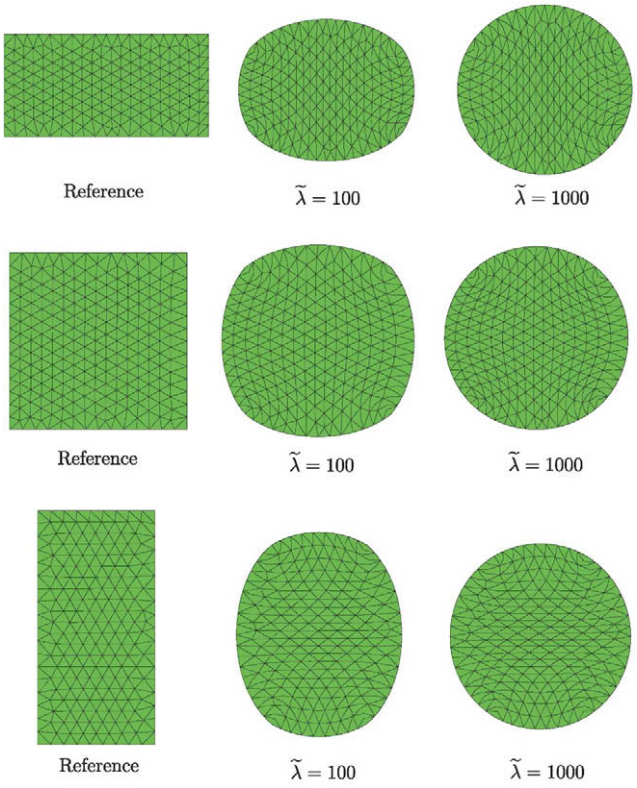

Fig. 12. A model rectangle to show surface effects.

mid-node and the upper edge is constrained only in horizontal direction at the mid-node. For the whole boundary the material parameter $\tilde{\mu} = 0$ is assumed. For the bulk, the Lamé parameters

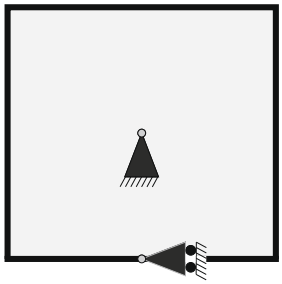

Fig. 13. A model square to show anisotropic surface effects.

are assumed to be $\bar{\mu} = 10$ and $\bar{\lambda} = 1000$. The effects of the boundary potential for different values of $\tilde{\lambda}$ is illustrated in Fig. 12. This example, clearly, shows that the surface tension effect tends to transfer a body into a circle and by increasing the surface tension effect this circle shrinks to a point.

6.6. First illustration of anisotropic surface tension type boundary effects

In this example a model square, as shown in Fig. 13, is considered. The model square is fixed in the center. It is also constrained in the horizontal direction on the bottom edge at the mid point. For the bulk, the Lamé parameters are assumed to be $\bar{\mu} = 10$ and $\bar{\lambda} = 100$. The anisotropic effects of the boundary potential for $\tilde{\lambda} = 50$ is illustrated in Fig. 14 for the boundary material model proposed in 5.4 and for different values of the material parameter $\tilde{\alpha}$. The unit vector $\boldsymbol{e} = (0, 1)$ is chosen which means that the anisotropic effects will be maximum where the curve tangent is vertical and will vanish where the curve tangent is horizontal.

6.7. Second illustration of anisotropic surface tension type boundary effects

In this example the same model square, as shown in Fig. 13, is considered. The model square is fixed in the center. It is also constrained in the horizontal direction on the bottom edge at the mid point. For the bulk, the Lamé parameters are assumed to be $\bar{\mu} = 10$ and $\bar{\lambda} = 100$. The anisotropic effects of the boundary potential for $\tilde{\lambda} = 50$ is illustrated in Fig. 15 for the boundary material model proposed in 5.4 and for the material parameter $\tilde{\alpha} = 1$. The unit vector $\mathrm{e} = (\sin\theta, \cos\theta)$ is chosen and the results corresponding to different values for θ are depicted.

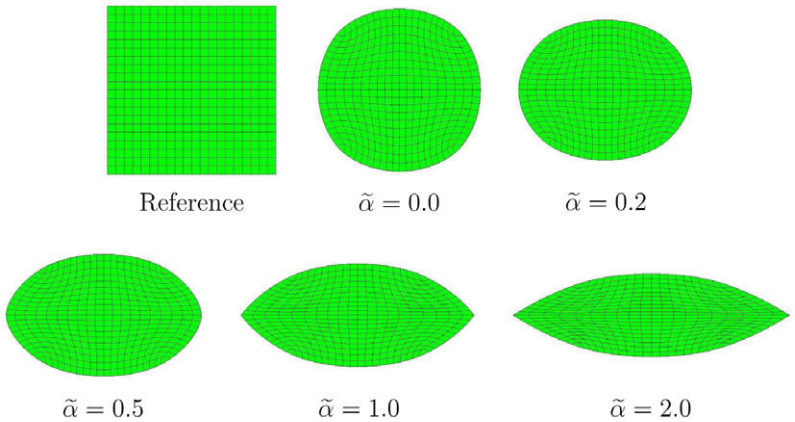

Fig. 14. Deformation of a model square due to anisotropic surface effects.

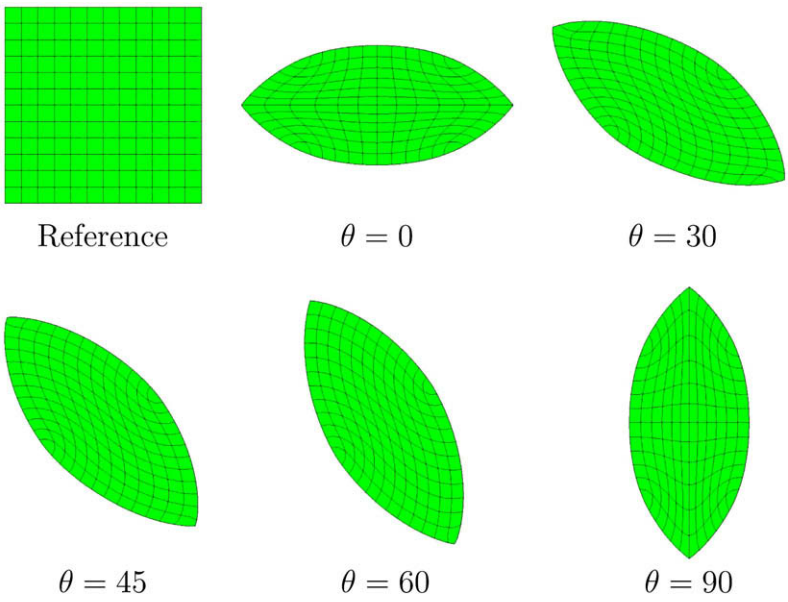

Fig. 15. Deformation of a model square due to anisotropic surface effects.

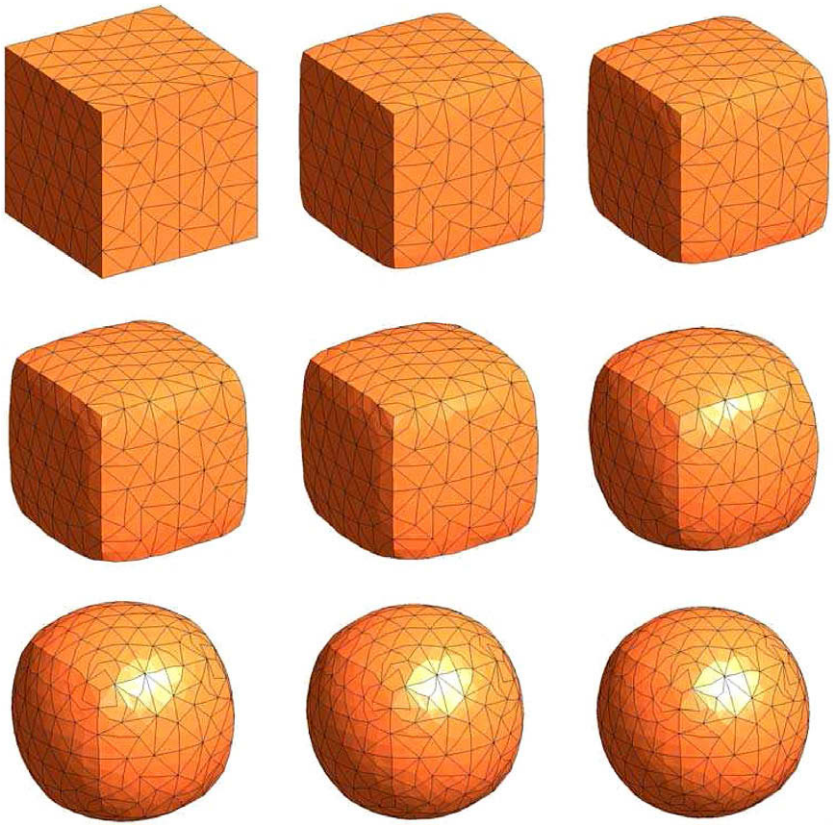

Fig. 16. Transformation of a cube to sphere due to surface effects.

6.8. A 3D example to illustrate the surface tension type boundary effects

In order to demonstrate the outlook of the present work in three-dimensional case, the next example as shown in Fig. 16 is considered. In order to limit the surface effects to the contributions coming from isotropic surface tension model, the material parameter contributing to the neo-Hookean resistance or anisotropic effects are set to zero. The effects of the boundary potential for the increasing value of surface tension is illustrated in Fig. 16. This example resembles the result shown in Fig. 12, however, in 3D. The implications of the three-dimensional finite element framework will be elaborated in the upcoming work.

7. Summary

A finite element framework for continua with boundary potentials has been presented. Based on geometry and kinematics of boundaries from the Dirichlet principle of minimum potential energy, the corresponding principle of virtual work accounting for contributions from boundary is derived. The discretized form of the principle of virtual work is given which provides a suitable framework for finite element implementation. Several models for boundary potentials are introduced and various numerical examples have been provided, which confirms the excellent efficiency of the proposed scheme. The solution procedure is robust and shows the asymptotically quadratic rate of convergence for Newton–Raphson scheme.

The extension of the proposed scheme to the three-dimensional case in presence of anisotropy will be the subject of forthcoming contributions.

References

[1] N.K. Adam, The Physics and Chemistry of Surfaces, Oxford University Press, London, 1941.
[2] M.E. Gurtin, A continuum theory for elastic material surfaces, Arch. Ration. Mech. Anal. 112 (1975) 97–160.
[3] M.E. Gurtin, A. Murdoch, A continuum theory of elastic material surfaces, Arch. Ration. Mech. Anal. 57 (1975) 291–323.
[4] E.M. Lifshitz, L.D. Landau, Fluid Mechanics, Course of Theoretical Physics, second ed., vol. 6, Butterworth-Heinemann, 1987.
[5] P.H. Leo, R.F. Sekerka, The effect of surface stress on crystal–melt and crystal–crystal equilibrium, Acta Metall. 37 (1989) 3119–3138.
[6] P.H. Leo, R.F. Sekerka, The effect of elastic fields on the morphological stability of a precipitate grown from solid solution, Acta Metall. 37 (1989) 3139–3149.
[7] Erwin Kreyszig, Differential Geometry, Dover Publications, 1991.
[8] F. Gruttmann, R.L. Taylor, Theory and finite element formulation of rubberlike membrane shells using principal stretches, Int. J. Numer. Methods Engrg. 35 (1992) 1111–1126.
[9] Jerrold E. Marsden, Thomas J.R. Hughes, Mathematical Foundations of Elasticity, Dover Publications, 1994.
[10] L. Olson, E. Kock, A variational approach for modelling surface tension effects in inviscid fluids, Comput. Mech. 14 (2) (1994) 140–153.
[11] K.J. Bathe, Finite Element Procedures (Part 1–2), second ed., Prentice Hall, 1995.
[12] W. Adamson, A.P. Gast, Physical Chemistry of Surfaces, Wiley-Interscience, 1997.
[13] S.E. Navti, K. Ravindran, C. Taylor, R.W. Lewis, Finite element modelling of surface tension effects using a Lagrangian–Eulerian kinematic description, Comput. Methods Appl. Mech. Engrg. 147 (1997) 41–60.
[14] N.K. Simha, K. Bhattacharya, Equilibrium conditions at corners and edges of an interface in a multiphase solid, Mater. Sci. Eng. A238 (1997) 32–41.
[15] N.K. Simha, K. Bhattacharya, Kinetics of phase boundaries with edges and junctions, J. Mech. Phys. Solids 46 (1998) 2323–2359.
[16] N.K. Simha, K. Bhattacharya, Kinetics of phase boundaries with edges and junctions in a three-dimensional multiphase body, J. Mech. Phys. Solids 48 (2000) 2619–2641.
[17] WC. Johnson, Superficial stress and strain at coherent interfaces, Acta Mater. 48 (2000) 433–444.
[18] T.J.R. Hughes, The Finite Element Method: Linear Static and Dynamic Finite Element Analysis, Dover Publications, 2000.
[19] Michel Bellet, Implementation of surface tension with wall adhesion effects in a three-dimensional finite element model for fluid flow, Commun. Numer. Methods Engrg. 17 (8) (2001) 563–579.
[20] W. Haiss, Surface stress of clean and adsorbate-covered solids, Rep. Prog. Phys. 64 (2001) 591–648.
[21] W. Dettmer, P.H. Saksono, D. Perić, On a finite element formulation for incompressible newtonian fluid flows on moving domains in the presence of surface tension, Commun. Numer. Methods Engrg. 19 (9) (2003) 659–668.
[22] F.D. Fischer, N.K. Simha, J. Svoboda, Kinetics of diffusional phase transformation in multicomponent elastic–plastic materials, ASME J. Eng. Mater. Technol. 125 (2003) 266–276.
[23] E. Kuhl, H. Askes, P. Steinmann, An ale formulation based on spatial and material settings of continuum mechanics. Part 1: Generic hyperelastic formulation, Comput. Methods Appl. Mech. Engrg. 193 (2004) 4207–4222.
[24] E. Fried, M.E. Gurtin, AA unified treatment of evolving interfaces accounting for small deformations and atomic transport with emphasis on grain-boundaries and epitaxy, in: H. Aref, E. Van der Giessen (Eds.), Advances in Applied Mechanics, 40 (2004) 1–177.
[25] G. Kaptay, Classification and general derivation of interfacial forces, acting on phases, situated in the bulk, or at the interface of other phases, J. Mater. Sci. 40 (2005) 2125–2131.
[26] P. Steinmann, O. Häsner, On material interfaces in thermomechanical solids, Arch. Appl. Mech. 75 (2005) 31–41.
[27] O.C. Zienkiewicz, R.L. Taylor, The Finite Element Method for Solid and Structural Mechanics, sixth ed., Butterworth-Heinemann, 2005.
[28] P.G. Ciarlet, An Introduction to Differential Geometry with Applications to Elasticity, Springer, 2006.
[29] W. Dettmer, D. Perić, A computational framework for free surface fluid flows accounting for surface tension, Comput. Methods Appl. Mech. Engrg. 195 (23–24) (2006) 3038–3071.
[30] P.H. Saksono, D. Perić, On finite element modelling of surface tension. Variational formulation and applications—Part I: quasistatic problems, Comput. Mech. 38 (2006) 265–281.
[31] P.H. Saksono, D. Perić, On finite element modelling of surface tension. Variational formulation and applications—Part II: dynamic problems, Comput. Mech. 38 (2006) 251–263.
[32] F. Yang, Effect of interfacial stresses on the elastic behavior of nanocomposite materials, J. Appl. Phys. 99 (2006) 054306.
[33] D. Kramer, J. Weissmüller, A note on surface stress and surface tension and their interrelation via Shuttleworth's equation and the Lippmann equation, Surf. Sci. 601 (2007) 3042–3051.
[34] J. Mosler, M. Ortiz, Variational h-adaption in finite deformation elasticity and plasticity, Int. J. Numer. Methods Engrg. 72 (5) (2007) 505–523.
[35] J. Mosler, A novel variational algorithmic formulation for wrinkling at finite strains based on energy minimization: application to mesh adaption, Comput. Methods Appl. Mech. Engrg. 197 (2007) 1131–1146.
[36] J. Bonet, R.D. Wood, Nonlinear Continuum Mechanics for Finite Element Analysis, second ed., Cambridge University Press, 2008.
[37] F.D. Fischer, T. Waitz, D. Vollath, N.K. Simha, On the role of surface energy and surface stress in phase-transforming nanoparticles, Prog. Mater. Sci. 53 (2008) 481–527.
[38] P. Steinmann, On boundary potential energies in deformational and configurational mechanics, J. Mech. Phys. Solids 56 (3) (2008) 772–800.
[39] G. Yun, H.S. Park, A multiscale, finite deformation formulation for surface stress effects on the coupled thermomechanical behavior of nanomaterials, Comput. Methods Appl. Mech. Engrg. 197 (2008) 3337–3350.